Cement & Concrete Composites 30 (2008) 603–611

Contents lists available at ScienceDirect

Cement & Concrete Composites

journal homepage: www.elsevier.com/locate/cemconcomp

Bond strength prediction for reinforced concrete members with highly corroded reinforcing bars

Lan Chung [a], Jang-Ho Jay Kim [b], Seong-Tae Yi [c,*]

[a] Department of Architectural Engineering, Dankook University, 147, Hannam-Dong, Yongsan-gu, Seoul-si 140-714, South Korea
[b] Department of Civil and Environmental Engineering, Yonsei University, 134 Shinchon-dong, Seodaemun-gu, Seoul-si 120-749, South Korea
[c] Department of Civil Engineering, Chung Cheong University, 330, Wolgok-ri, Kangnae-myun, Cheongwon-kun, Chungbuk-do 363-792, South Korea

ARTICLE INFO

Article history:
Received 2 November 2006
Received in revised form 24 March 2008
Accepted 25 March 2008
Available online 11 April 2008

Keywords:
Bond properties
Corrosion
Reinforced concretes
Pre-corrosion
Post-corrosion

ABSTRACT

Due to the shortage of natural fine aggregates in many countries, sea sand has been alternatively used in the production of concrete. However, due to the presence of chlorides in sea sand, the threat of corrosion of steel reinforcing bars embedded in such concrete has become a major concern. Therefore, many studies related to corrosion level and bond behavior have been performed. The realistic corrosion levels at which the aged structures are exposed to danger are usually greater than 1% and beyond minimal 2%. Since safety predictions of aged concrete structures based on corrosion failure are of the utmost importance, research concerning more realistic corrosion levels would help the prediction process. For this purpose, two types of specimens are investigated to understand the bond properties as a function of corrosion level in RC members. Prismatic concrete specimens with reinforcements subjected to corrosion before and after casting of concrete are used for pullout tests. Based on the experimental data, an equation for bond strength prediction is developed. Also, the validity of the proposed equation is demonstrated through comparison with the existing prediction curves.

1. Introduction

Corrosion of reinforcement is a major contributing factor to the deterioration of reinforced and prestressed concrete structures. More specifically, structures exposed to seawater and chloride-containing chemicals are more vulnerable to corrosion. In some instances, aggregates, primarily fine aggregates, contaminated with chlorides have been used in the concrete, resulting in rapid corrosion of the reinforcement. Also, reinforcement used for many reinforced concrete (RC) structures is exposed to moisture in the air causing slight corrosion even before casting of concrete. Due to the increasing prevalence of corrosion in RC structures, the problem of repair and rehabilitation of existing structures is becoming a major part of construction works. The estimate for repair and rehabilitation of transportation infrastructure in the US exceeds several billion dollars [1]. To plan repair strategies for damaged structures, the strength of the existing structures needs to be estimated. Currently, much research [2–9] has focused on the factors affecting the corrosion level of reinforcement in concrete. Relatively less information, however, is available on the behavior of structural members that have corroded reinforcement.

Results available in the literature focus on: (1) techniques for measuring the amount of corrosion [10,11]; (2) comparison of laboratory and field corrosion level studies [12]; (3) use of corrosion-reducing admixtures as a constituent for new concrete [13], and penetration admixtures for existing structures to reduced the rate of corrosion [14]. Available bond behavior results deal usually with low corrosion levels in which reinforcement mass loss is less than 1% [15]. However, the realistic corrosion levels at which the aged structures are exposed to danger are usually greater than 1% and beyond minimal 2% [16–19]. Since the prediction of the safety of aged concrete structures based on corrosion failure is of the utmost importance, research concerning more realistic corrosion levels is presently needed. Also, most of the studies performed on corrosion problems have concerned corrosion levels obtained by synthetic means, such as through electric current-induced accelerated corrosion, either before or after casting of the concrete. However, there have not been any studies to correlate the results from these pre- and post-corrosion methods where the data can be used to predict the safety of concrete structure based on corrosion level. Because of the limitations of the currently available data on corrosion level, a study that can resolve these difficulties is needed to better predict the safety of aged concrete structures due to corrosion.

As an overall perspective of corrosion research, a study dealing with both pre-corrosion and post-corrosion is planned. Pre-corrosion method is considered not only to obtain corrosion, but also to compare with and normalize the pre-existing corrosion data for overall evaluation of safety of concrete structures due to corrosion level. Post-corrosion method is used to evaluate the corrosion

* Corresponding author. Tel.: +82 43 230 2315; fax: +82 43 230 2319.
E-mail address: yist@ok.ac.kr (S.-T. Yi).

0958-9465/$ - see front matter © 2008 Elsevier Ltd. All rights reserved.
doi:10.1016/j.cemconcomp.2008.03.006

level in more realistic setting conditions where the structural corrosion problems occur in reinforcements embedded in concrete under confined condition. However, the difficulty associated with the post-corrosion method is that the corrosion level is difficult to control, especially the desired maximum corrosion level is practically unobtainable. Since this study focuses on the overall evaluation of safety of concrete structures based on corrosion level, the data from pre-existing corrosion studies, as well as newly obtained corrosion data from both pre- and post-corrosion methods, should be used to develop relations for concrete structure safety evaluation covering a wide range of corrosion levels.

In order to qualitatively and quantitatively understand the effects of corrosion on the bond properties in RC members, two types of bar pullout tests are made using prismatic concrete specimens. For the first specimen type, the reinforcing bars are pre-corroded before casting. The reinforcing bar of the second specimen type is corroded after concrete casting. Both methods used electric current to accelerate corrosion of the reinforcing bars.

Various corrosion levels up to 10% are applied to pre- and post-corroded bars for the preparation of pullout tests. The amount of corrosion is expressed as percentage of mass loss in comparison to the control bar. After the effective corrosion is applied, pullout tests are performed on both types of specimens. The major tasks consisted of (1) designing bond specimen geometry; (2) finding an efficient way to apply maximum and consistent corrosion along the entire length of steel bar before casting of concrete (pre-corroded) and after casting concrete (post-corroded); and (3) obtaining bond properties that can be used to predict the behavior of RC structural elements with corroded reinforcement. It was expected that specimens would fail by splitting of concrete. The following sections describe the logic used for producing reinforcement corrosion, specimen selection, test procedure, discussions and results.

2. Current-induced corrosion process

As mentioned previously, two types of electric current-induced accelerated corrosion were performed on reinforcing steel bars. Figs. 1 and 2 are schematic diagrams of the current-induced accelerated corrosion setup of steel bars before (pre-corrosion) and after casting of concrete (post-corrosion), respectively. The magnitude of corrosion was measured using percentage of mass loss. A method developed for inducing corrosion by externally applied electric current was used for this study. An electric current is passed from the reinforcement to the copper plate placed inside of 3% NaCl solution underneath the corroding steel bar as shown in Figs. 1 and 2. This copper plate acts as a cathodic site, which consumes

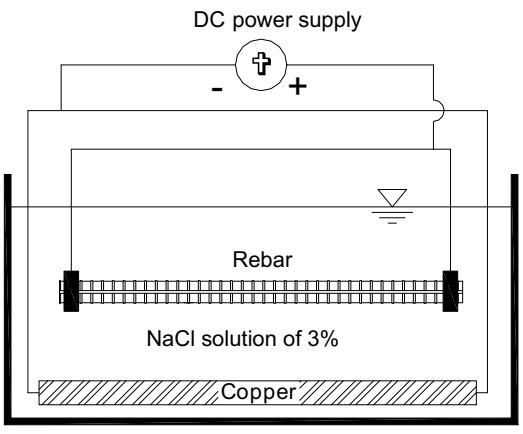

Fig. 1. Current-induced corrosion setup of bare steel bar (pre-corrosion).

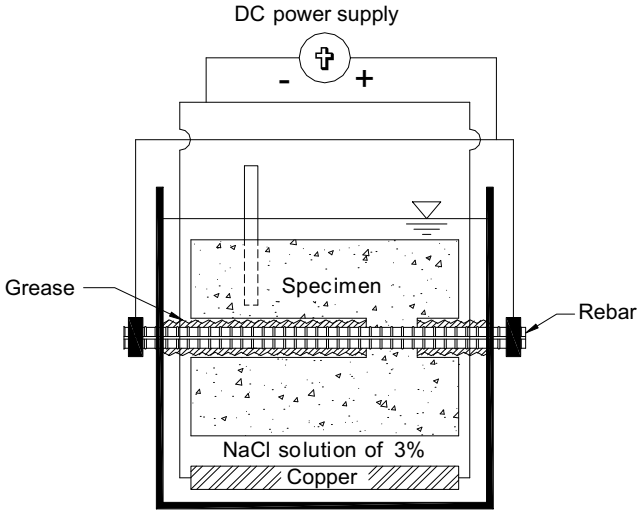

Fig. 2. Current-induced corrosion setup of concrete cast steel bar (post-corrosion).

the electrons given out by the corroding deformed bar. Generally, μm/year (mpy) is used to represent corrosion level and remaining service life of an aged RC member. However, in this study, the focus is to achieve maximum corrosion level, rather than the corrosion amount based on the applied electric current.

A power supply with an output of 24 V DC and 12 amps was used to induce the corrosion. The positive terminal was connected to the deformed bar whereas the negative terminal was connected to the copper plate. In the case of post-corroded steel bars, both end portions are placed outside of the tank containing the salt solution to prevent the corrosion of exposed bar and at the junction of concrete. This setup worked well, which is confirmed by the presence of fairly uniform corrosion along the bar when the specimens are checked after the pullout test. After the power supply was turned on, the current flowing through the system was recorded at a 1 min interval using a computer-controlled data-acquisition system. The amount of corrosion is related to the electrical energy consumed, which is a function of voltage, amperage, and time interval. The amount of corrosion can be estimated from

$$\text{mass loss} = \frac{\text{time (s)} \times \text{current (A)} \times 55.847}{2 \times 96,487} \quad (1)$$

The quantity of charge applied for any given electrolysis is given by the product of time (s) and current (A). For the corrosion process, for each mol of iron that oxidizes, 2 mols of electrons are given out, consuming a charge of $2 \times 96{,}487$ coulomb. The mass loss is then calculated by multiplying the applied charge (C) by the molar mass (55.847 g/mol for iron) and dividing by the charge needed per mole.

3. Measurement of mass losses

After the completion of the pullout test, the corroded bars were removed from the specimens and the cleaned bar was weighed and the total percentage loss was determined. An attempt was made to obtain the mass losses along the length of the bar to ascertain the uniformity of corrosion. The setup shown in Fig. 3 was used for the measurement. Method of rust cleaning followed the procedure specified in ASTM G 1-72 "Preparing, cleaning, and evaluating corrosion test specimens [20]." Archimedes's principle was used to obtain the mass loss for every 6 mm length of the bar. After the bar was cleaned, starting from corroded end, 6 mm segments were marked using a scribe. Then the bar was mounted on the stand using a grip and placed on an electronic scale. Water is filled up

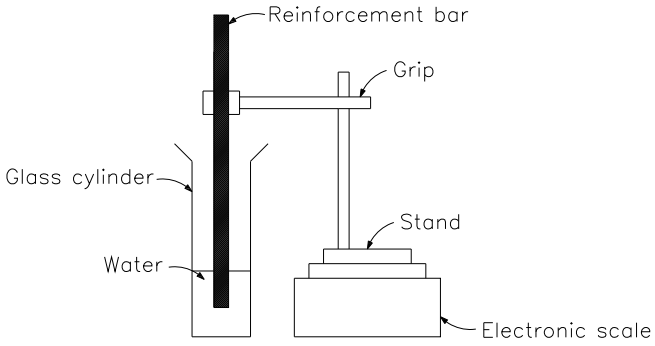

Fig. 3. Setup for mass loss measurement.

to the first mark, which is 6 mm from bottom (or corroded) end and the change in mass was recorded. This step was continued until the water reached 126 mm mark. The procedure was also repeated for the uncorroded or control bar. The comparison of mass change between control and corroded bar provided the mass loss for every 6 mm. The mass losses were added to obtain the cumulative mass loss.

4. Test specimens and experimental program

4.1. Test specimen

Various types of specimens have been used for bond tests such as the commonly used specimen in ASTM C 234 [21] and modified beam tests. ASTM specifies that the concentric pullout test can be used only for comparison purposes. The details of various other test setups can be found in the research report by Chapman and Shah [22]. After evaluating various setups, a modified version of the setup proposed in Danish Standard DS 2082 [23] was used for the current study (Fig. 4).

The specimen consisted of a concrete prism in which a single piece of mild steel bar is embedded in the center (Fig. 4). Other than the $3d_b$ length of steel bar in contact with concrete, the rest of the steel bar is placed inside of embedded PVC pipe so that the steel bar is not in contact with concrete. The bond length was chosen as $3d_b$ to ensure bond failure. The bond failure is associated with splitting cracking, because the slip of rebar within concrete specimen causes tensile strain around the circumference of rebar, causing splitting cracks. Therefore, a $3d_b$ bond length provides sufficient bonding between concrete and rebar until slippage of rebar occurring at sufficient loading. The dimensions of the concrete cross-sections were chosen to prevent tension failure of concrete. The molds were constructed using 13 mm thick ply-wood, coated with several layers of water repellent to avoid water penetration to wood. The photograph of the setup is shown in Fig. 5. Two sets of three screws were threaded into the pipe to align and grip the ends of the deformed bars. This arrangement ensured location and alignment of the steel bar. Extra plates with openings slightly larger than the bar size were placed at the ends of the mold to avoid leakage of mortar concrete into the hollow pipes. A minimum of three compression cylinders were cast for each bond specimen. Compression cylinders with a dimension of 100 × 200 mm, usually employed in the compressive strength test, were cast to obtain the compressive behavior of concrete.

4.2. Materials and mixture proportion

The constituent materials consisted of ASTM Type I cement, concrete, sand, 9 mm maximum size coarse aggregate, tap water, chloride based accelerating admixtures, and air-entraining admixtures. The expected 28-day compressive strength of the concrete is 25.0 MPa. An air-entraining admixture was used to simulate the concrete used in outside environments, while a chloride admixture was used to aid corrosion. The water–cement ratio (w/c) was 0.58. A high w/c was used to facilitate rapid corrosion. Table 1 shows the mixture proportion of concrete. D13 (13 mm) reinforcing bars are used. The yield and tensile strengths of the bars were 384.7 MPa and 526.8 MPa, respectively.

4.3. Mixing, casting, and curing

A concrete mixer with a maximum capacity of 0.3 m^3 was used for the mixing. First, coarse and fine aggregates and 2/3 of the water were loaded into the mixer and mixed for 1 min to allow for absorption of water. Then, cement, remaining water, and the admixtures were added, and the contents were mixed for 3 min. After a rest period of 3 min, mixing continued for an additional 2 min.

Before mixing the concrete, the mass of the reinforcement for each specimen was recorded and the bars were aligned and fastened to the molds. A mold-releasing chemical was applied to the inside surface of both pullout specimen molds and cylinder molds. A table vibrator was used for compaction of both pullout specimens and cylinders. At the end of casting, polyethylene sheets were used to cover the samples for the next 24 h.

When the specimens were water cured after the first 24 h for 28 days, it was found that it was almost impossible to induce uniform corrosion on the pullout bar. Because the water permeability of concrete is low, there is always more corrosion at the junction of the bar and concrete. Therefore, the procedure described in Section

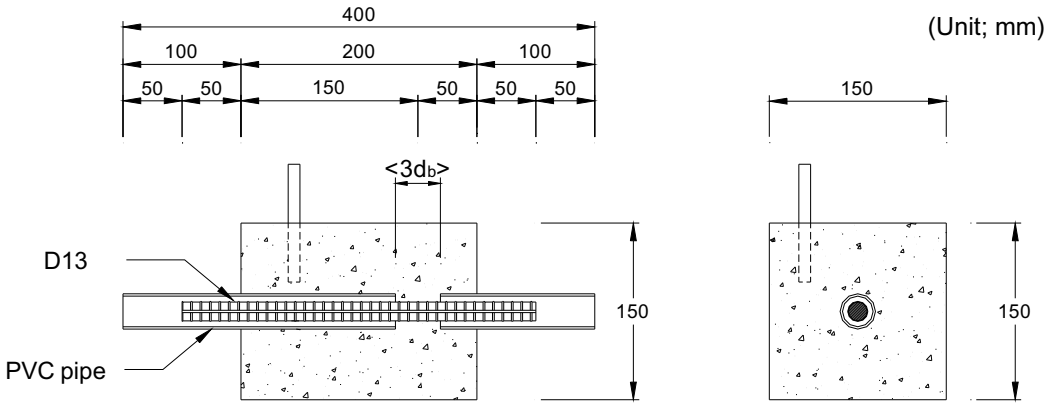

Fig. 4. Pullout test specimen dimensions.

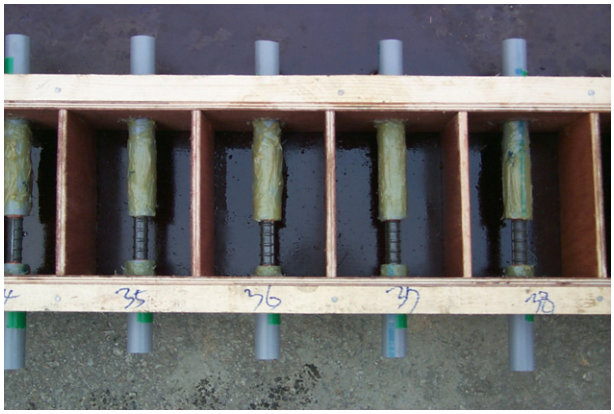

Fig. 5. Photo of pullout specimen molds.

4.5 was chosen based on tests of both pullout specimens and cylinders.

4.4. Conditioning specimens

After 24 h from casting, the samples were demolded and immediately placed in 3% NaCl solution. Because the concrete was not yet in fully hardened state and a considerable amount of pore water was present, it was possible to induce corrosion along the bar by induced current. Current-induced corrosion was started after the specimens were soaked in saltwater for a minimum of 3 days.

4.5. Test procedure

The test setup for the pullout test is shown in Fig. 6. The pullout load was applied as a compression load at the shorter end of steel bar from the $3d_b$ segment. The longer end of steel bar was attached with 5 mm linear variable displacement transducer (LVDT) to measure the bond-slip response between the concrete and the reinforcing bar (Fig. 6). The test was conducted using a 534 kN capacity universal testing machine. Because the $3d_b$ length of the steel bar in contact with concrete is located closer to the load application point, the stable longitudinal slippage failure of the bar is ensured by using the $3d_b$ segment of the specimens. None of the bars reached yield point during the tests. The companion cylinders were tested in compression using the standard ASTM C 39 procedure [24].

5. Test results

For each pre-corroded and post-corroded specimen type, three specimens are prepared for experiments. Specimens are designated as J13-L-M, where J is assigned either A for post-corrosion, B for pre-corrosion, or S for no corrosion; L is an expected corrosion level 0%, 2%, 3%, 4%, 5%, 7%, or 10%; and M for corrosion is an achieved corrosion level, except when there is no corrosion (i.e., J = S) where M for no corrosion is assigned a specimen number I, II, or III.

5.1. Achieved corrosion levels

Initially the desired corrosion levels for both pre- and post-corroded specimens were 2%, 3%, 4%, 5%, 7%, and 10% of its original

Table 1
Concrete mixture proportion

Target strength (MPa)	w/c ratio (%)	Weight of mix ingredients (kg/m^3)						Slump (cm)	Average compressive strength (MPa)
		Water	Cement	Sand	Aggregate	Air-entraining (A/E) admixture	Accelerating admixture		
25.0	58	185	319	690	991	1.6	9.6	15	28.3

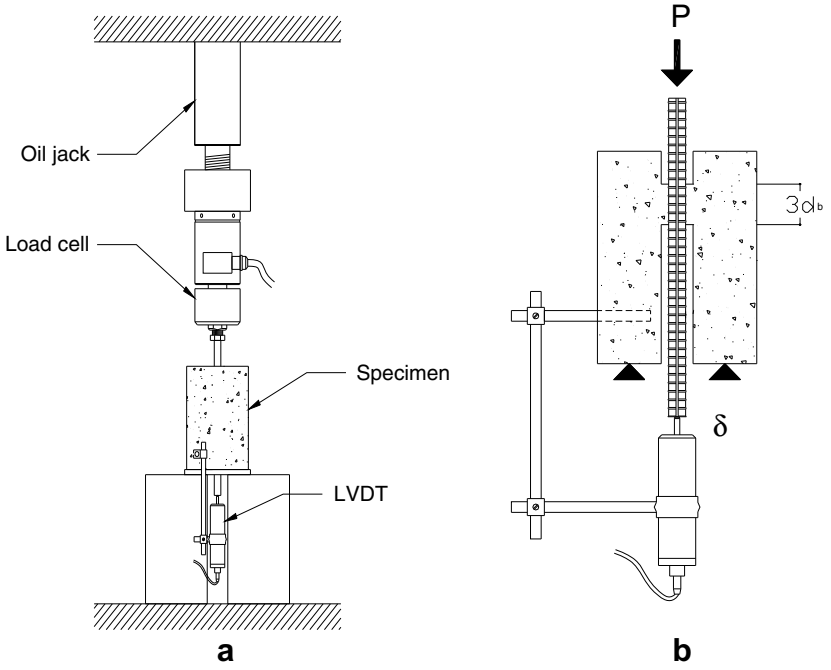

Fig. 6. (a) Global pullout test setup; and (b) pullout test setup of loading point.

cross sectional area of the reinforcement. However, the achieved corrosion levels are very different than the expected corrosion level in most of the specimens. As shown in Tables 2 and 3, the achieved corrosion levels for pre- and post-corroded specimens are far less than the expected corrosion levels in most specimens except in several specimens. In pre-corroded specimens, the achieved corrosions are approximately 75% of the expected corrosion level in the specimens with the expected corrosion level less than or equal to 4%. However, as the expected corrosion level increases the achieved corrosion levels become approximately 50% of the expected corrosion values of greater than or equal to 5%. In post-corroded specimens, the achieved corrosion levels are approximately less than 2% for most of the specimens no matter what the expected corrosion levels are. This trend indicates that the application of corrosion using electric current-induced method is not efficient and that the post-corroded application is more difficult than in pre-corroded application. The goal of this study is not measuring corrosion level using electric current-induced method, but it is to develop a concrete structure safety evaluation based on corrosion level. So no matter what the corrosion levels came out to be, the achieved corrosion levels are used for the analysis.

5.2. Corrosion crack pattern

The typical crack pattern of specimens with corroded bars tested in this study is shown in Fig. 7. It is important to note that when the loading is applied, a crack is initiated nearby the loading point and subsequently propagating to a direction parallel to the reinforcing bar. From the experiments, it is also observed that when the corrosion level is relatively a large value, the number of cracks is less but they are more localized and have wider crack widths. However, when the corrosion level is relatively a small

Table 2
Test results of pre-corroded specimens (pre-corrosion)

Expected corrosion level (%)	Achieved corrosion level (%)	Specimen designation	Max. load (kN)	Bond length (mm)	Max. bond strength (MPa)	Slip at max. load (mm)
0	0.0	S13-0-I	21.78	37.1	14.7	0.53
	0.0	S13-0-II	24.82	36.6	17.0	0.80
	0.0	S13-0-III	21.29	37.9	14.0	0.58
2	1.5	B13-2-1.5	23.35	38.3	15.2	0.34
	1.6	B13-2-1.6	24.43	36.9	16.6	0.80
	2.1	B13-2-2.1[a]	27.17	37.9	18.0	0.95
3	2.2	B13-3-2.2	23.94	38.4	15.6	0.94
	2.3	B13-3-2.3	25.41	38.0	16.7	1.06
	2.4	B13-3-2.4	23.25	37.8	15.4	0.57
4	2.4	B13-4-2.4	22.66	37.2	15.2	0.48
	2.5	B13-4-2.5	24.53	38.1	16.1	1.08
	2.8	B13-4-2.8	23.74	38.0	15.6	0.37
5	2.7	B13-5-2.7	24.53	36.9	16.6	1.06
	3.1	B13-5-3.1	21.78	37.4	14.4	0.49
	3.2	B13-5-3.2	22.96	37.1	15.5	0.71
7	3.4	B13-7-3.4	18.25	36.8	12.4	0.95
	4.1	B13-7-4.1[a]	20.01	35.9	13.9	0.92
	8.8	B13-7-8.8	13.64	36.0	9.4	1.31
10	4.6	B13-10-4.6	15.30	36.6	10.5	1.25
	5.7	B13-10-5.7	14.13	36.9	9.5	1.17
	6.3	B13-10-6.3[a]	19.62	38.4	12.8	1.39

[a] Excluded from data due to loading eccentricity, problems in cutting steel bars, etc.

Table 3
Test results of post-corroded specimens (post-corrosion)

Expected corrosion level (%)	Achieved corrosion level (%)	Specimen designation	Max. load (kN)	Bond length (mm)	Max. bond strength (MPa)	Slip at max. load (mm)
0	0.0	S13-0-I	21.78	37.1	14.7	0.53
	0.0	S13-0-II	24.82	36.6	17.0	0.80
	0.0	S13-0-III	21.29	37.9	14.0	0.58
2	0.1	A13-2-0.1	29.92	37.2	20.1	0.18
	0.5	A13-2-0.5	25.80	37.1	17.4	0.61
	1.0	A13-2-1.0	30.02	37.4	20.0	0.08
3	1.1	A13-3-1.1[a]	21.48	37.0	14.5	0.62
	1.2	A13-3-1.2	23.64	36.7	16.2	0.03
	1.4	A13-3-1.4	26.59	37.1	17.9	0.03
4	0.9	A13-4-0.9	24.82	38.0	16.4	0.06
	2.5	A13-4-2.5[a]	32.28	39.1	20.6	0.05
	0.2	A13-4-0.2[a]	23.54	37.0	15.9	0.55
5	0.8	A13-5-0.8	27.27	36.7	18.5	0.06
	1.9	A13-5-1.9	30.12	37.1	20.3	0.06
	0.9	A13-5-0.9[a]	20.90	37.1	14.1	0.39
7	0.5	A13-7-0.5[a]	24.33	36.5	16.7	0.68
	1.4	A13-7-1.4[a]	28.06	37.0	19.0	0.03
	2.2	A13-7-2.2	21.68	37.8	14.4	0.76
10	0.6	A13-10-0.6[a]	23.25	36.1	16.1	0.55
	0.7	A13-10-0.7[a]	22.07	35.9	15.4	0.49
	1.9	A13-10-1.9	23.35	36.8	15.9	0.03

[a] Excluded from data due to loading eccentricity, problems in cutting steel bars, etc.

value, the number of cracks is greater, but they are distributed along the member and have smaller crack widths.

5.3. Load–slip curves

Fig. 8 shows the relationship between load and the slip obtained at the longer end of steel bar by LVDT with achieved corrosion level on each reinforcing bar. It is important to recognize the following information from this figure: (a) the point of stiffness change after formation of initial crack; and (b) slips corresponding to maximum and yielding loads.

5.4. Bond strength and slip

The bond strength has been calculated using the initial (uncorroded) cross-sectional dimension of the bars. From the experiment, it was observed that the corrosion started at the rib section of the bars. As the corrosion continued, the rib height declined. When the corrosion level reached 2%, the rib no longer existed or only small portion remained. This is the reason why 2% corrosion level is the critical corrosion level effecting bond strength.

The bond strength of corroded bar f_b is calculated as

$$f_b = \frac{P}{l_b \sum_0} \tag{2}$$

where P is pullout load; l_b is bond length; and $\sum_0$ is bar initial circumference.

The effective bond length of D13 corroded bars was 38.1 ± 2.1 mm ($3d_b$). Tables 2 and 3 tabulate the pullout experimental results of pre-corroded and post-corroded bars for various corrosion levels, respectively. Both tables also include the pullout test results of non-corroded bars. It is important to note that the achieved corrosion levels of steel bars were less than the expected corrosion levels due to lose of applied electric current to the surrounding environment during the accelerated corrosion process. Also, the achieved corrosion levels for post-corroded specimens are less than pre-corroded specimens when compared to the expected corrosion levels. This trend is expected since the application of corrosion in steel bars cast in concrete is much more difficult compared to bare steel bars. This is due to the dispersion of electric currents during the application of corrosion.

For S13 specimens, initial slip of steel bars occurred at the bond strengths of 7.1–10.3 MPa. Slip displacements of 0.53–0.80 mm are measured at the bond strengths of 14.0–17.0 MPa. Initial slip of steel bars for pre-corroded and post-corroded specimens occurred at 2.9–10.3 MPa and 7.5–19.9 MPa, respectively. Also, slip displacements of 0.34–1.31 mm for pre-corroded specimens are measured at the bond strengths of 9.4–16.7 MPa. For pre-corroded specimens, the slip displacement tended to increase as the pre-corrosion level increased. In the case for post-corroded specimens, slip displacements of 0.03–0.76 mm are measured at the bond strengths of 14.4–20.3 MPa. For post-corroded specimens, the slip displacement at the maximum pullout load tended to decrease until the achieved post-corrosion level reached 2% and then started to increase after 2% corrosion level.

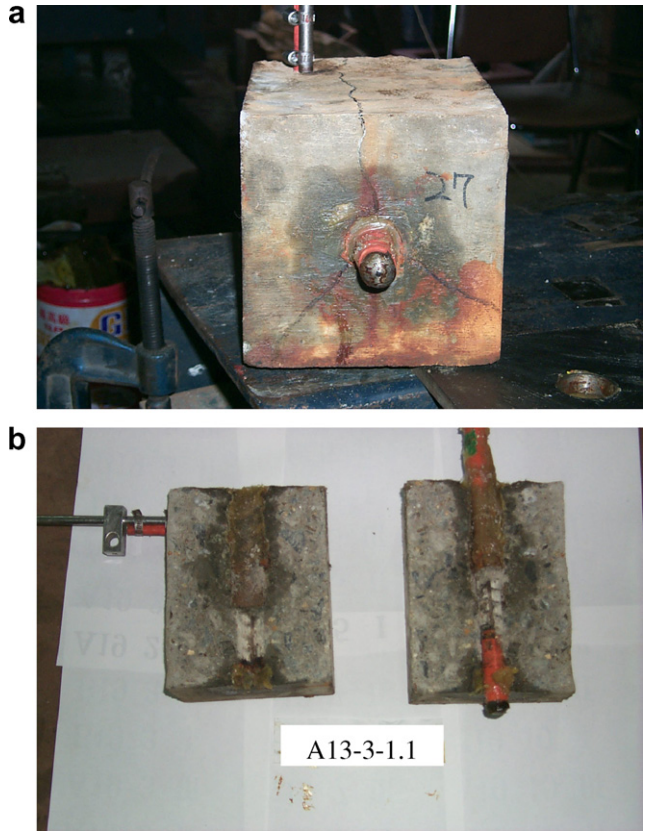

Fig. 7. Typical cracked specimen with corroded bar: (a) Exterior view; and (b) split view.

6. Discussions of analysis results

6.1. General behaviors

In this study, the authors have performed numerous experiments to apply corrosion on reinforcing bars using the accelerated electric current induced corrosion method. However, the amount of expected corrosion level was practically unobtainable for post-corrosion. Also, the reference studies to obtain the bond strength data with large corrosion level using this corrosion method were performed without success. Therefore, using the limited number of pre- and post-corroded specimen data obtained from this study, the bond prediction curve is developed. Then, the developed curve is compared with other bond prediction curves as a function of corrosion level reported by other researchers. It is important to note that the pre- and post-corrosion specimens gave sufficient range of corrosion level up to 8.8% for bond strength evaluation based on corrosion level. Also, the pre- and post-corrosion specimens represent application of corrosion under laboratory and in situ settings, which are important in design bond strength prediction curves for concrete structures with corrosion damage.

Figs. 9 and 10, respectively, show calculated bond strength and slip at bond strength versus achieved corrosion level using current-induced corrosion method. The general trend of bond strength curves of both pre-corroded and post-corroded specimens is similar: the bond strength initially increases up to a maximum value, but decreases afterward. Also, the bond strengths of pre-corroded specimens are less than those of post-corroded specimens.

In Fig. 9, the prediction curve of bond strength as a function of corrosion level is compared with other bond strength models. The curve shows that the bond strength values are higher than other models until the corrosion level of 3%. Beyond 3% corrosion level, the bond strength is less than other proposed models. However, the relative differences between the newly proposed curve and existing curves are small and within the range of acceptable variation. The significant difference between the prediction curves is that the behavior of newly proposed model is initially horizontal until 2% corrosion level and decreasing nonlinearly beyond 2%. This trend has been observed in the study reported by Chung et al. [25]. The other models are just a declining straight line with constant slope. Therefore, the newly proposed prediction curve can be

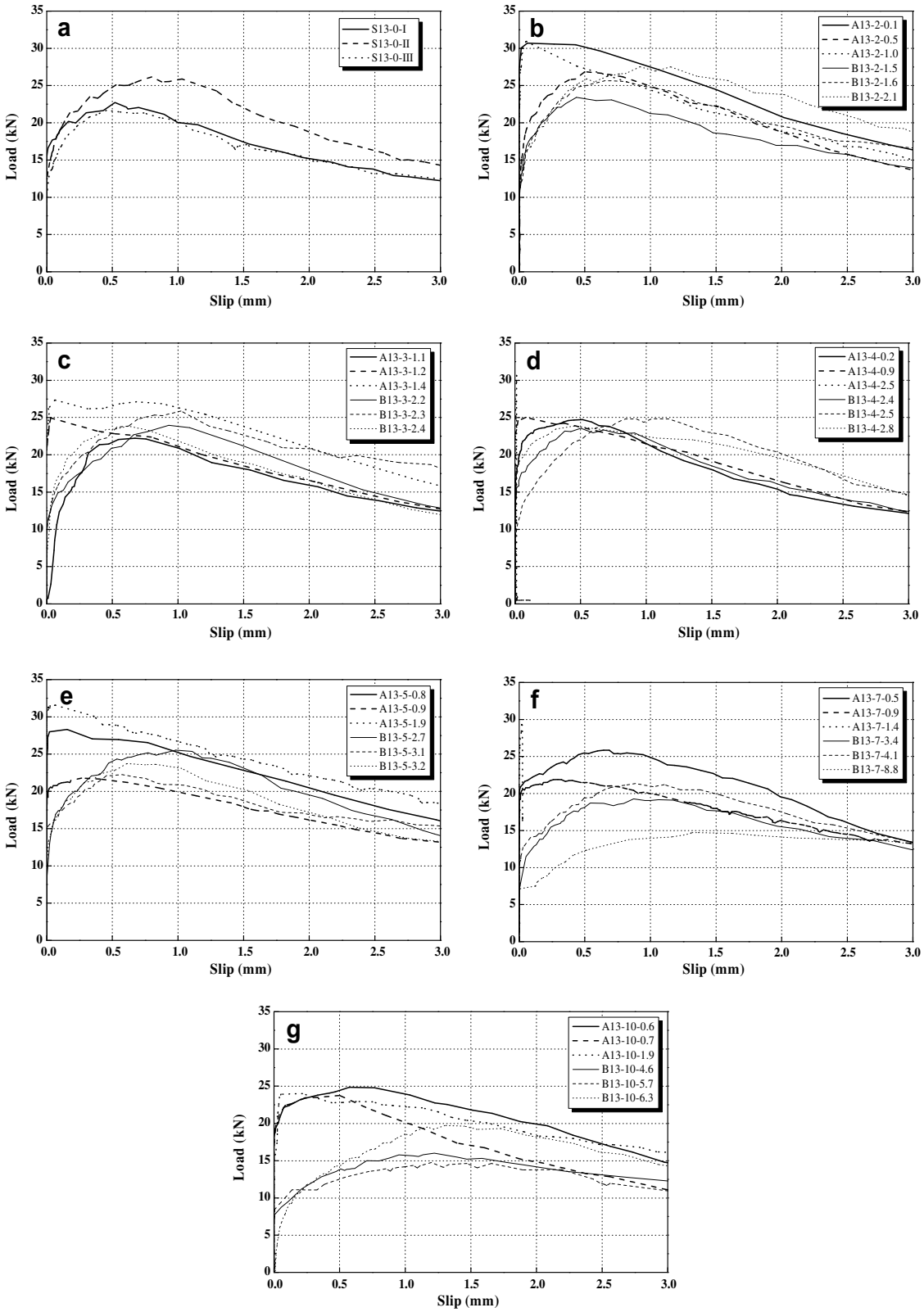

Fig. 8. Load–slip curves with expected corrosion level: (a) No corrosion specimens; (b) 2% corroded specimens; (c) 3% corroded specimens; (d) 4% corroded specimens; (e) 5% corroded specimens; (f) 7% corroded specimens; and (g) 10% corroded specimens.

considered more realistic and show the actual bond strength behavior. The bond strength prediction behavior of this trend has been already reported by many researchers, where the corrosion up to 2% shows increase in bond strength and declines beyond 2%. However, the increase in bond strength up to 2% corrosion is negligible and can be considered to be constant, especially when the prediction curve is used for safety design or performance evaluation of concrete structure with corrosion.

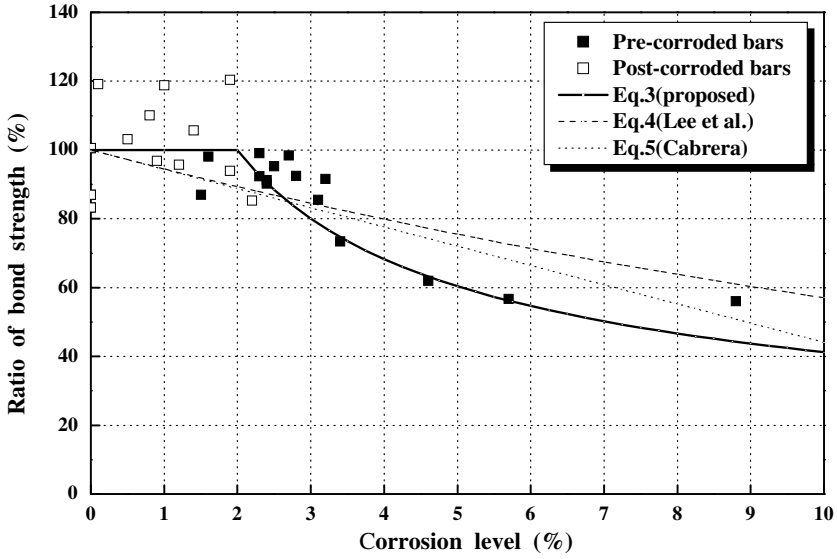

Fig. 9. Bond strength versus achieved corrosion level using current-induced corrosion method.

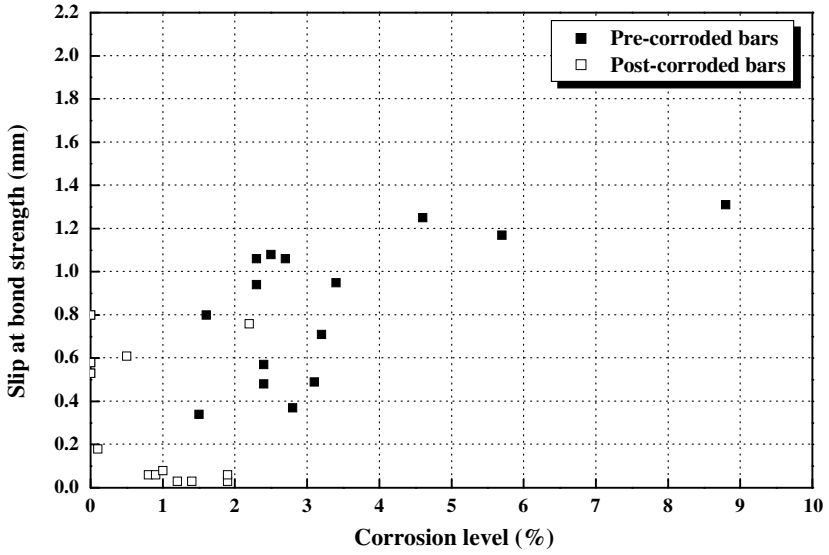

Fig. 10. Slip at bond strength versus achieved corrosion level using current-induced corrosion method.

6.2. Proposed bond strength model

The bond strength Eq. (3) as an exponential function is obtained from the LSM regression analyses on the test data obtained from this study.

$$\begin{array}{ll} u_b = 16.87 & \text{for } C_0 \leqslant 2.0 \\ \text{or} 24.7C_0^{-0.55} & \text{for } C_0 > 2.0 \end{array} \quad (3)$$

where u_b is bond strength and C_0 is corrosion level in %.

From the reference study, several researchers [19,26] reported the empirical equations of bond strength as a function of corrosion level as the following two equations. Lee et al. [19] proposed the bond strength as an exponential function with corrosion level as a variable, which is expressed as

$$u_b = 5.21e^{-0.0561C_0}\ (\text{MPa}) \quad (4)$$

where u_b is bond strength and C_0 is corrosion level. Cabrera [26] proposed the bond strength as a function of corrosion level as

$$u_b = 23.478 - 1.313C_0(\text{MPa}) \quad (5)$$

In Fig. 9, the comparison of the experimental data and the bond strength equation explained in Eq. (3), and the empirical bond strength equations reported by other researchers (i.e., Eqs. (4) and (5)) is shown. Fig. 9 clearly shows that the previous empirical equations predict bond strength to decline linearly as corrosion level increases, which does not properly capture the gradual bond strength reduction behavior after 2% corrosion level. Also, for corrosion levels less than and greater than 2%, the previous empirical bond strength equations underestimate and overestimate bond strengths, respectively. However, the newly proposed equation correctly and properly predicts the bond strength for the corrosion level considered in the study.

7. Conclusions

1. The general trend of bond strength curves of both pre-corroded and post-corroded specimens is similar: the bond strength initially increases up to a maximum value, but eventually

decreases for greater levels of corrosion. Also, the bond strengths of pre-corroded specimens are less than those of post-corroded specimens.

2. The proposed bond strength equation shows that the bond strength values are higher than those of other models until a corrosion level of 3%. Beyond 3% corrosion level, the bond strength becomes less than that given by the other referenced models. However, the relative differences between the newly proposed curve and existing curves are small and within the range of acceptable variation.
3. The significant difference between the newly proposed model and the previous prediction curves is in the shape of the curves, where the new model shows a more realistic behavior. For corrosion levels less than and greater than 2%, the previous empirical bond strength equations underestimate and overestimate bond strengths, respectively. Further studies on the bond characteristics of concrete structures with large corrosion levels over 3% are needed.

Acknowledgements

The authors wish to acknowledge the financial support of the Korea Science and Engineering Foundation (KOSEF) for the National Research Laboratory (NRL) project M01-0203-00-0068. The third author also wishes to thank the partial financial support of the project "Development of Intelligent Port and Logistics System for Super-Large Container Ships," which was sponsored by Ministry of Maritime and Fishery in Korea. These supports are deeply appreciated.

References

[1] McDonald DB. Design options for corrosion protections. Concrete 95 toward better concrete structures, Brisbane, Australia, 4–7 September 1995; p. 1–9.
[2] Gulikers JJW. Experimental investigations on macrocell corrosion in chloride-contaminated concrete. HERON 1996;41(2):107–23.
[3] Lopez W, Gonzalez JA. Influence of the degree of pore saturation on the resistivity of concrete and the corrosion rate of steel reinforcement. Cement Concrete Res 1993;23(2):368–76.
[4] Xiao C. Corrosion of reinforcement in concrete and number theory simulation. PhD thesis, Tsinghua University; 1996.
[5] Glass GK, Page CL, Short NR. Factors affecting the corrosion rate of steel in carbonated mortars. Corros Sci 1991;32(12):1283–94.
[6] Gonzalez JA, Lopez W, Rodriguez P. Effects of moisture availability on corrosion kinetics of steel embedded in concrete. Corrosion 1993;49(12):1004–10.
[7] Naish CC, Harker A, Carney RFA. Concrete inspection: Interpretation of potential and resistivity measurements. In: Page CL, Treadaway KWJ, Bamforth PB (Editors), Corrosion of Reinforcement in Concrete Society of Chemical Industry. 1990; p. 314–32.
[8] Arya C. Influence of cathode-to-anode area ratio and separation distance on galvanic corrosion currants of steel in concrete containing chlorides. Cement Concrete Res 1995;25(5):989–98.
[9] Alonso C, Andrade C, Gonzalez JA. Relation between resistivity and corrosion rate of reinforcements in carbonated mortar made with several cement types. Cement Concrete Res 1988;18(5):687–98.
[10] Scannell WT, Sohanghpurwala AA, Islam M, Babaei K, Purvis RL. Instructor Guide: SHRP Workshop on Physical assessment and design and treatment methodology for concrete bridge components relative to reinforcement corrosion. Publication No. FHWA-SA-97-041, HTA-20/3-97(500) QE, US Department of Transportation, Federal Highway Administration; December 1996.
[11] Berke NS, Shen DF, Sundberg KM. Comparison of the polarization resistance technique to macrocell corrosion technique. In: Berke NS, Chaker V, Whiting D, editors. Corrosion rates of steel in concrete. ASTM STP 1065. Philadelphia: American Society for Testing and Materials; 1990. p. 38–51.
[12] El-Jazairi B, Berke NS. The use of calcium nitrite as a corrosion inhibiting admixture to steel reinforcement in concrete. In: Page CL, Treadaway KWJ, Bamforth PB, editors. Corrosion of reinforcement in concrete. London: Elsevier Applied Science; 1990. p. 571–85.
[13] Dinakar P, Babu KG, Santhanam M. Corrosion behaviour of blended cements in low and medium strength concretes. Cement Concrete Compos 2007;29(2):136–45.
[14] Berke NS, Hicks MC, Hoopes RJ. Condition assessment of field structures with calcium nitrite. Concrete Bridges in Aggressive Environments, SP-151, Weyers RE, editors, American Concrete Institute, Farmington Hills, Mich., 1994; p. 43–71.
[15] Fu X, Chung DDL. Effect of water–cement ratio, curing age, silica fume, polymer admixtures, steel surface treatments, and corrosion on bond between concrete and steel reinforcing bars. ACI Mater J 1998;95(6):725–34.
[16] Clifton JR. Prediction the service life of concrete. ACI Mater J 1993;90(6):611–7.
[17] Mangat PS, Molloy BT. Prediction of long-term chloride concentration in concrete. Mater Struct 1994;27(4):338–46.
[18] Chung L, Najm H, Balaguru P. Flexural behavior of concrete slabs with corroded bars. Cement Concrete Compos 2008;30(3):184–93.
[19] Lee HS, Noguchi T, Tomosawa F. Evaluation of the bond properties between concrete and reinforcement as a function of the degree of reinforcement corrosion. Cement Concrete Res 2002;32(8):1313–8.
[20] ASTM G 1-72. Standard practice for preparing, cleaning, and evaluating corrosion test specimens. West Conshohocken (PA): American Society for Testing and Materials.
[21] ASTM C 234-01. Standard test method for comparing concretes on the basis of the bond developed with reinforcing steel. Annual book of ASTM standards. Philadelphia: American Society for Testing and Materials; 1991.
[22] Chapman RA, Shah SP. Early-age bond strength in reinforced concrete. ACI Mater J 1987;84(6):501–10.
[23] Danish Standards Organization, Pullout Test. DS 2082, Copenhagen, 1980, p. 2.
[24] ASTM C 39-01. Standard test method for compressive strength of cylindrical concrete specimens. Annual book of ASTM standards. Philadelphia: American Society for Testing and Materials; 2001.
[25] Chung L, Cho SH, Kim JHJ, Yi ST. Correction factor suggestion for ACI development length provisions based on flexural testing of RC slabs with various levels of corroded reinforcing bars. Eng Struct 2004;26(8):1013–26.
[26] Cabrera JG. Deterioration of concrete due to reinforcement steel corrosion. Cement Concrete Compos 1996;18(1):47–59.